Antiviral Research 164 (2019) 81–90

Contents lists available at ScienceDirect

Antiviral Research

journal homepage: www.elsevier.com/locate/antiviral

Novel influenza inhibitors designed to target PB1 interactions with host importin RanBP5

Gregory Mohl[a,*], Nathan Liddle[a], Joseph Nygaard[b], Alexander Dorius[a], Nathan Lyons[b], Jan Hodek[c], Jan Weber[c], David J. Michaelis[b,**], David D. Busath[a,***]

[a] Department of Physiology and Developmental Biology, Brigham Young University, Provo, UT 84602, USA
[b] Department of Chemistry and Biochemistry, Brigham Young University, USA
[c] Institute of Organic Chemistry and Biochemistry of the CAS, Prague, Czech Republic

ARTICLE INFO

Keywords:
Virtual screening
Antiviral
Nuclear localization
Polymerase inhibition

ABSTRACT

In search of novel targets for influenza inhibitors, a site on PB1 was selected for its high conservation and probable interaction with a host protein, RanBP5, that is key to nuclear import of PB1, where it complexes with PB2, PA, and NP to transcribe viral RNA. Docking with libraries of drug-like compounds led to a selection of five candidates that bound tightly and with a pose likely to inhibit protein binding. These were purchased and tested *in vitro*, found to be active, and then one was synthetically expanded to explore the structure-activity relationship. The top candidates had a carboxylic acid converted to an ester and electron-withdrawing substituents added to a phenyl group in the original structure. Resistance was slow to develop, but cytotoxicity was moderately high. Nuclear localization of PB1 and *in vitro* polymerase activity were both strongly inhibited.

1. Introduction

The influenza virus infects hundreds of thousands annually in the United States, costing billions in direct medical costs alone (Molinari et al., 2007). Drug development is crucial for influenza because resistance can develop against therapeutics, such as occurred globally between 2006 and 2009 for the M2 blockers amantadine and rimantadine (Dong et al., 2015), and seasonal influenza can escape current vaccines (Hensley, 2014). Neuraminidase (NA) inhibitors are one type of antiviral treatment options in the United States for influenza infection, but resistance to NA inhibitors has been demonstrated and remains a major concern (Hussain et al., 2017; McKimm-Breschkin, 2000). Another is baloxavir marboxil, a cap-dependent endonuclease inhibitor that was approved last year for use in Japan and the United States (Noshi et al., 2018). Baloxavir is a potent inhibitor of influenza virus replication, but recent work has shown that resistance is still a concern (Jones et al., 2018). Several other classes of inhibitors are currently in clinical development and could someday supplement NA inhibitors (McKimm-Breschkin et al., 2018; Perwitasari et al., 2014). A combination antiviral therapy to prevent resistance development, similar to the multi-drug therapy used against HIV, is an important aim of developing novel influenza inhibitors (Hoopes et al., 2011).

Host-pathogen interactions play important roles in viral modulation of the host immune response and pathogenesis. Influenza is a unique RNA virus because it replicates in the nucleus. The nuclear pore complex (NPC) prevents non-specific proteins from accumulating in the nucleus. Fodor et al. have shown that nuclear accumulation of polymerase basic 1 (PB1) is dependent on the formation of a trimeric complex with polymerase acidic (PA) and Ran-binding protein 5 (RanBP5), a host nuclear import factor (Fig. 1) (Fodor and Smith, 2004; Hutchinson et al., 2011). In the absence of PA, nuclear accumulation of PB1 was significantly perturbed. Similarly, mutations that destabilized the interaction between PB1/PA and RanBP5 significantly reduced nuclear localization of PB1 and effectively prevented viral replication in tissue culture (Hutchinson et al., 2011). This nuclear import mechanism is distinct from the import of incoming viral ribonucleoprotein complexes (vRNPs) at the beginning of an infection, which is RanBP5-independent (Hutchinson and Fodor, 2013; Wu and Panté, 2009).

Because of the conserved and essential nature of the PB1 nuclear import mechanism, blocking nuclear localization of influenza virus proteins is a potentially promising mechanism of new antivirals. Many other attempts at blocking nuclear import or export have been documented, but most have targeted host proteins (Chase et al., 2008; Perwitasari et al., 2014; Resa-Infante et al., 2015). In one case,

* Corresponding author.
** Corresponding author.
*** Corresponding author.
E-mail addresses: greg.mohl@ucsf.edu (G. Mohl), dmichaelis@byu.edu (D.J. Michaelis), david_busath@byu.edu (D.D. Busath).

https://doi.org/10.1016/j.antiviral.2019.02.003
Received 7 August 2018; Received in revised form 30 January 2019; Accepted 3 February 2019
Available online 08 February 2019
0166-3542/

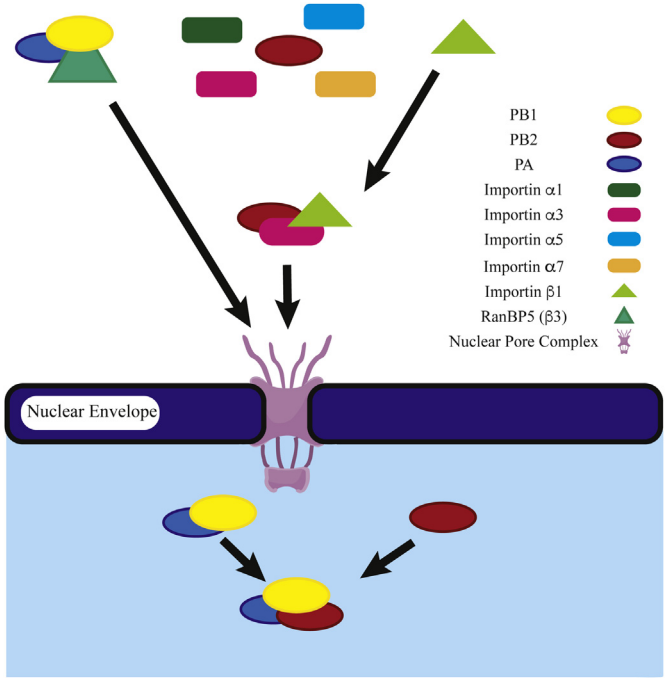

Fig. 1. Mechanism of IAV Polymerase Nuclear Import. PB1/PA associates with RanBP5, which shuttles them into the nucleus as a heterodimer. PB2 binds to Importin α1, α3, α5, or α7, which then binds to Importin β1. The full polymerase complex (PB1/PA/PB2) associates in the nucleus, where it carries out its function.

disrupting a host factor essential for influenza replication in mice, importin-alpha7, lead to a resistant strain that was more virulent than the wild-type in as few as five passages (Resa-Infante et al., 2015). Several groups have also independently identified PB1 blockers that prevent replication by destabilizing PB1-PA interactions, PB1-PB2 interactions, or by unknown mechanisms, though resistance and solubility are still concerns with these compounds (Desantis et al., 2017; Li et al., 2017; Massari et al., 2016; Ortigoza et al., 2012; Su et al., 2010). One group showed that a PB1-PA interaction inhibitor blocked localization of PA to the nucleus (Muratore et al., 2012). Another group showed that targeting the PB1/PA interaction lead to the discovery of compounds with a high genetic barrier to resistance (Zhang et al., 2018).

The method of virtual screening for protein-protein interaction inhibitors (Busschots et al., 2012; Geppert et al., 2011, 2012; Shima et al., 2013) was used to identify possible PB1/PA:RanBP5 interaction inhibitors, which were purchased and tested in cell culture infection assays. Several derivatives of a top compound were synthesized and tested to determine the structure activity relationship of this inhibitor class. The mode of action was explored using confocal microscopy and a luciferase reporter assay for RNA-dependent RNA polymerase activity.

2. Methods

For more detailed methods, please refer to the Supplementary Data.

2.1. Docking

Autodock Vina (Trott and Olson, 2010) and Glide (Friesner et al., 2004, 2006; Halgren et al., 2004) were used to screen compounds for relative binding affinities at the proposed binding site. 4WSB was used for docking (Reich et al., 2014). ClusPro was used to dock 3W3Z and 4WSB to develop a model for PB1/PA:RanBP5 complexation (Comeau et al., 2004; Kobayashi and Matsuura, 2013; Kozakov et al., 2017).

2.2. Immunofluorescence (IF) assay

As described previously (Kolocouris et al., 2014), Madin-Darby canine kidney epithelial (MDCK) cells were seeded onto glass coverslips, infected with trypsin-activated virus, and incubated at 33 °C for 16 h. Coverslips were washed, fixed with cold acetone, and stained with anti-influenza A or anti-influenza B fluorescein isothiocyanate (FITC)-labeled monoclonal antibody (Millipore, Billerica, MA). Infected cells were counted with a fluorescent microscope. The 50%-effective concentrations (EC_{50}) were obtained by a non-linear least-squares fit in KaleidaGraph (Synergy Software, Reading, PA, USA).

2.3. Cytotoxicity assays

Cells are seeded into the 60 internal wells of a 96-well plate. After 48 h, growth media is replaced with media containing test compound. The cells were incubated with the test compounds for 72 h at 37 °C in a humidified 5% CO_2 incubator. Crystal violet (Schmidtke et al., 2001) or XTT (Scudiero et al., 1988; Wutzler et al., 2002) was used to determine cytotoxic activity. The cells were washed, stained, lysed, and then the optical density was measured. The 50%-cytotoxic concentrations (CC_{50}) were obtained by a non-linear least-squares fit in KaleidaGraph (Synergy Software, Reading, PA, USA) or Prism 7.04 (GraphPad, La Jolla, CA, USA).

2.4. Cytopathic Effect (CPE) assays

Cells were seeded into the 60 internal wells of a 96-well plate. About 50x$TCID_{50}$ of activated virus was added to each well. The growth media was replaced with Dulbecco's Modified Eagle's Medium (DMEM) supplemented with 0.2 μg/ml of TPCK-treated trypsin, and the appropriate dose of test compound was added to each well. The plates were incubated for approximately 72 h. Crystal violet (Schmidtke et al., 2001) or XTT (Scudiero et al., 1988; Wutzler et al., 2002) was used to determine the CPE. The EC_{50}, or the concentration of test compound that protected half of the cells, was calculated using a non-linear least squares fit in KaleidaGraph or Prism 7.04. Cases where the culture was protected less than 50% before cytotoxicity became dominant as inhibitor concentrations were increased were designated “No effect.”

2.5. Plaque assay

Cells were seeded into plates and incubated overnight. The growth media was replaced with test medium, and the test compounds were added to the cells. After one hour, the cells were infected with influenza A H1N1 virus with a multiplicity of infection (MOI) of 0.005. After another hour, the medium in the wells was overlaid with 1.25% Avicel (FMC BioPolymer). After 72 h, the cells were washed with PBS and fixed with 4% paraformaldehyde for 30 min at 4 °C. The cells were washed again with PBS after fixation and were stained with Giemsa stain. Pictures from the microscope were recorded, and the area of survived cells was calculated using ImageJ. The EC_{50}, or the concentration of test compound that reduced the plaque area by 50%, was calculated using non-linear regression analysis in Prism 7.04.

2.6. Resistance testing

The procedure described in Kolocouris et al. was used to determine the resistance profile (Kolocouris et al., 2014).

2.7. Polymerase inhibition assay

Flu polymerase activity was measured using the Dual-Glo® Luciferase Assay System (Promega Corporation, Madison, WI). 293T cells were transfected using Lipofectamine 2000 with plasmids containing genomic sequences for the three influenza A H1N1 polymerase

subunit proteins (PA, PB1, PB2), nucleoprotein (NP), and fragment-encoding firefly luciferase (pPolI). The IC_{50} was calculated using non-linear regression analysis in Prism 7.04.

2.8. Localization assay

MDCK cells treated with compound **20** and infected with influenza A/CA/07/2009 were imaged and scored to determine the localization of PB1 and NP. Importazole (IPZ) at 50 μM was used as a positive control for blocking nuclear accumulation of PB1 (Soderholm et al., 2011). Anti-PB1 antibodies (GTX125923, GeneTex, Irvine, CA) and AlexaFluor488-labeled secondary antibodies (A-110008, ThermoFisher, Eugene, OR) were used to detect cellular localization of PB1. Anti-NP antibodies (GTX125989, GeneTex, Irvine, CA) and AlexaFluor488-labeled secondary antibodies (A-110008, ThermoFisher, Eugene, OR) were used to detect cellular localization of NP. Cells were stained with 4′,6-diamidino-2-phenylindole (DAPI) Fluoromount-G (0100-20, Southern Biotech, Birmingham, AL) to detect the nuclei of the cells for comparison.

2.9. Imaging

Images were obtained on an Olympus Fluoview FV1000 microscope using the 40×/1.3 oil objective. Images were collected with 1600 by 1600 pixels at 8 μs/pixel. A 405 nm laser diode was used to excite DAPI, and a 488 nm Argon laser was used to excite AlexaFluor488. Analysis was performed in ImageJ. Uninfected controls and antibody controls were compared to untreated controls to determine appropriate thresholds for the background. Twice the average intensity of the signal in the nuclei and cytoplasm of uninfected cells was used as the background. The signal intensity of the nucleus and cytoplasm were measured in ImageJ, and the ratio of the nuclear signal over the cytoplasmic signal for each cell was used to classify the localization as nuclear, nucleocytoplasmic, or cytoplasmic (Hutchinson et al., 2011).

2.10. Sequence analysis

IAV and IBV sequences of PB1 were downloaded from the Influenza Research Database (fludb.org) on August 17th, 2016 and September 7th, 2016 respectively. The sequences were aligned using the multialign function from the Bioinformatics toolbox in MATLAB. After alignment, unique sequences were preserved, and the results were inspected visually. Microsoft Excel was used to analyze the aligned sequences. The frequency of the most conserved amino acid and the number of reported amino acids at each position were used to determine conservation at each position.

3. Results

3.1. Novel hits discovered using virtual screening

Using the IAV polymerase Protein Data Bank structure 4WSB, the Asinex (Winston-Salem, NC) protein-protein interaction library was docked with Glide (Schrödinger, Cambridge, MA) to a potential antiviral binding site (Fig. 2) near the bipartite nuclear localization signal (NLS) of PB1 and the predicted interface with RanBP5 (Friesner et al., 2004, 2006; Halgren et al., 2004; Reich et al., 2014).

The docking process was broken up into three stages, each with increasing precision (Fig. 3). The best conformations of the top 30 compounds from the initial virtual screen were visually scored, and eight compounds were selected for library expansion. Structure searches were performed on the Otava, Asinex, and Zinc websites for commercially available compounds similar to the eight compounds from the initial screen. This expansion resulted in a set of 3,216 readily available compounds similar to those identified in the initial screen. These were filtered through docking to identify five with the highest predicted binding scores.

Five compounds were selected and purchased from Asinex (Fig. 4). These compounds were screened against influenza virus using the immunofluorescence (IF) assay (Kolocouris et al., 2014). The compounds were also tested for cytotoxicity using a crystal violet cytotoxicity (CV-CTX) assay (Schmidtke et al., 2001). These commercially available compounds had low micromolar efficacy against influenza A virus (IAV) and had some activity against influenza B virus (IBV) (Table 1). Two of the compounds, LAS and ASN, have promising efficacy in the IF assay with 50% effective concentrations (EC_{50}'s) of 9.5 ± 0.7 μM and 15 ± 2 μM respectively against A/WS/33. The 50% cytotoxic concentrations (CC_{50}'s) for LAS and ASN are 389 ± 23 μM and 117 ± 20 μM, suggesting that there is a promising therapeutic window available for inhibitors that block influenza virus replication by this mechanism.

3.2. Structure-activity relationship of LAS analogs

LAS was selected for structure-activity relationship determination due to the relative ease and cost of synthesis and the favorable activity compared to the other compounds. Twenty-four derivatives of LAS were synthesized. The general synthesis involved epoxide opening, followed by nucleophilic substitution. The different derivatives were made by using different starting materials purchased from Combi-Blocks (San Diego, CA). These derivatives were characterized by mass spectrometry, NMR, and IR (Supplementary Data, Experimental Section). The derivatives were then tested against A/WS/33 (H1N1) (Fig. 5, Table 2). The compounds were initially tested in the IF, CV-CTX, and the crystal violet cytopathic effect (CV-CPE) (Schmidtke et al., 2001) assays to determine their efficacy and toxicity. Preliminary changes were made to the meta-substituted carboxylic acid moiety (R_2 in Fig. 5). Changing the carboxylic acid to a methyl ester, the position of the acid from meta-substituted to para-substituted, and extending the acid from the ring by a methylene resulted in a combined 100-fold improvement to the activity (compound **6,** Table 2). Subsequent modifications to the benzyloxy group (R_1 in Fig. 5) led to further improvements. Adding electronegative electron-withdrawing groups to the phenyl ring of the benzyloxy group (R_1 in Fig. 5) led to a further 10-fold increase in activity, resulting in an overall 1000-fold improvement in activity (compounds **20–22,** Table 2).

Four compounds were tested against five different influenza virus strains, including a strain of influenza B, in the IF (Table 3) and CV-CPE (Table 4) assays to determine the spectrum of activity against multiple strains. All four compounds showed activities comparable to those in A/WS/33 (from Table 2) against the other five strains tested. The differences were generally small between strains and large between inhibitors, suggesting that the binding site structure and mechanism of inhibition are similar in all species and that the inhibitors vary because of the impact of their structural differences on that site and inhibitory mechanism.

3.3. Mode of influenza inhibition

The resistance profile was determined by passaging the virus in the presence of an inhibitory concentration of the test compounds (Table 5). A/Victoria/3/75 was passaged ten times in the presence of ASN, beginning at 10 μM for passage zero (P0), and later for increasing dosages of ASN (see Methods). Passages five (P5) and ten (P10) were then tested in the IF assay. The compound showed a 2-fold reduction in efficacy against P5 and a 7-fold reduction against P10 relative to the efficacy measured against the wild type (P0). A/WS/33 was passaged ten times against compound **20**. Passaging began using 0.2 μM compound **20** (~IF EC_{50}) and was increased to 8 μM (the CV-CPE EC_{50}) by a factor of two each passage. P5 and P10 were tested against the compound in the IF assay to determine resistance development. In ten passages, no resistance was detected in the IF assay against compound

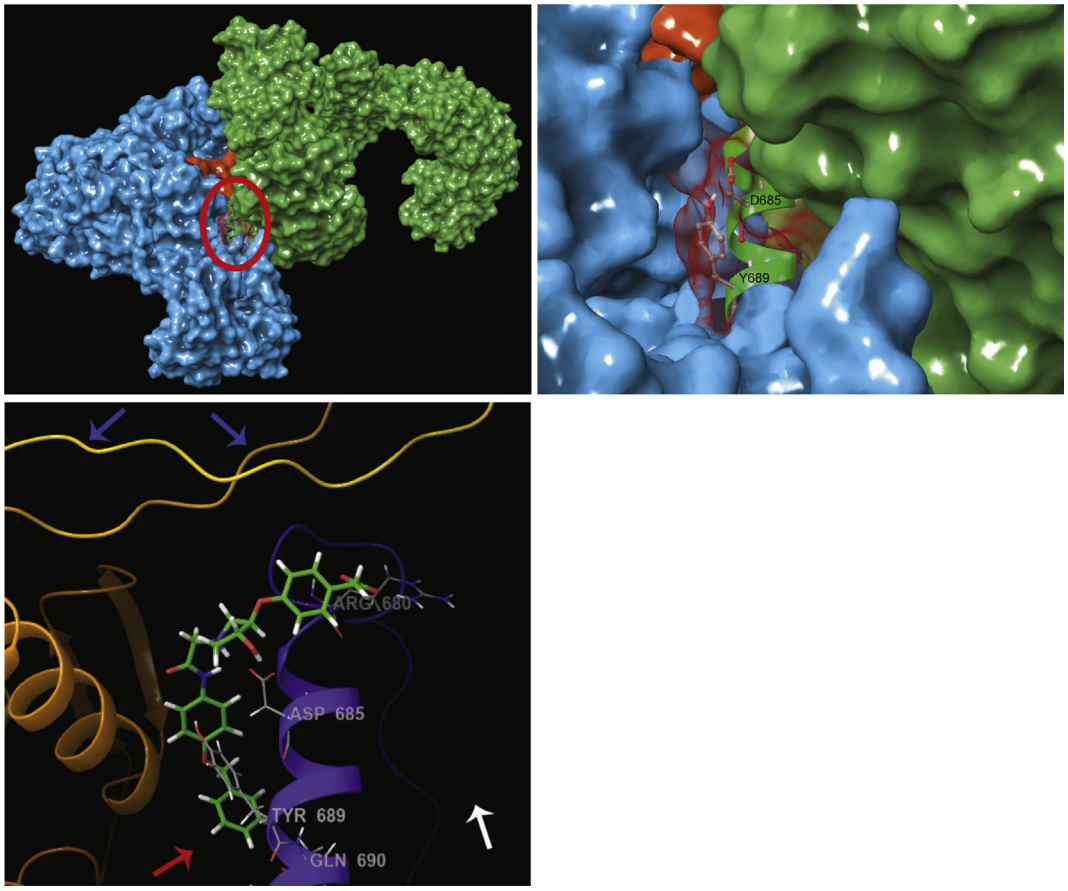

Fig. 2. Proposed Binding Site with Docked Ligand. A) PB1/PA (4WSB chains A,B; Blue surface) in complex with RanBP5 homologue Kap121p (3W3Z; Green Surface), with red oval showing the proposed inhibitor binding site. B) Blow up of the region of interest marked by the red oval in A. Key residues (D685 and Y689) are displayed with a transparent red surface and the ball and stick representation. The anchor helix (green ribbon) is important for PB1-RanBP5 interaction. C) View of the binding site with compound 5 docked. The bipartite nuclear localization signal (blue arrows), RanBP5 Binding interface (white arrow), and PB2 binding site (red arrow) are all proximal to the purported small molecule binding site. The anchor helix (purple ribbon) contains Y689, D685, and R680, which all have important interactions with the ligand. (For interpretation of the references to colour in this figure legend, the reader is referred to the Web version of this article.)

20. This contrasts with resistance formation within 1–2 passages found previously under similar conditions for amantadine (Kolocouris et al., 2014) or within 6 passages for Oseltamivir (Zhang et al., 2018).

The sequences of all IAV and IBV PB1 from the Influenza Research Database were compared using MATLAB. Only unique sequences were used in the analysis. The predicted binding site for these compounds was completely conserved in sequence across the four IAV strains tested here and partially conserved (45.5%) in IBV (Table 6). The crystal structures of the influenza polymerase for IAV (4WSB) and IBV (4WSA) were then compared to observe structural differences in the binding site. The aligned structures were very similar at the predicted antiviral binding site, with a few exceptions (Fig. 6). G681 is 99.9% conserved in IAV, but the corresponding position in IBV is an asparagine. N680 changes the way the helix turns relative to G681. D685 in IAV is 99.5% conserved, but E684 in IBV has an additional methylene group that causes the negatively charged carboxylate to extend into the pocket further. Our model of PB1/PA based on 4WSA shows that E684 can interact with K207, a residue on the NLS that is important for RanBP5

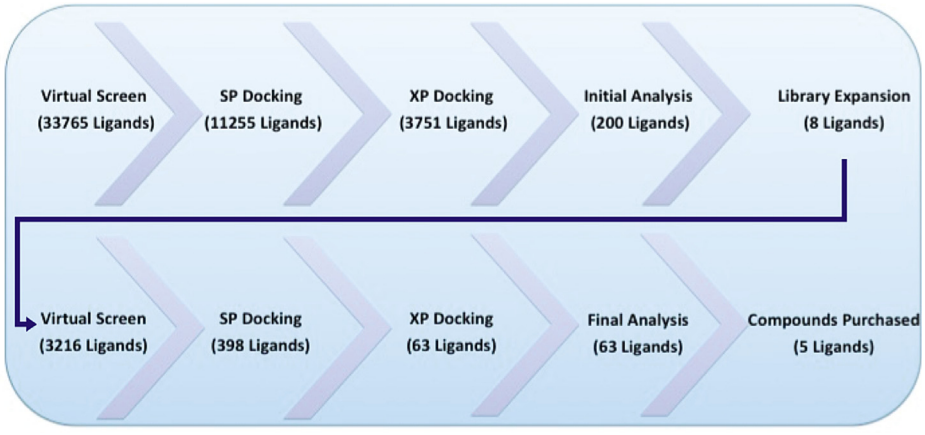

Fig. 3. Virtual Screening Workflow. A library of PPI inhibitors were docked to the binding site with progressively higher precision (Virtual Screen, SP = standard precision, XP = extra precision). Eight ligands were selected for library expansion via structure similarity searches. The docking procedure was repeated with the new library, and five compounds were selected for *in vitro* validation.

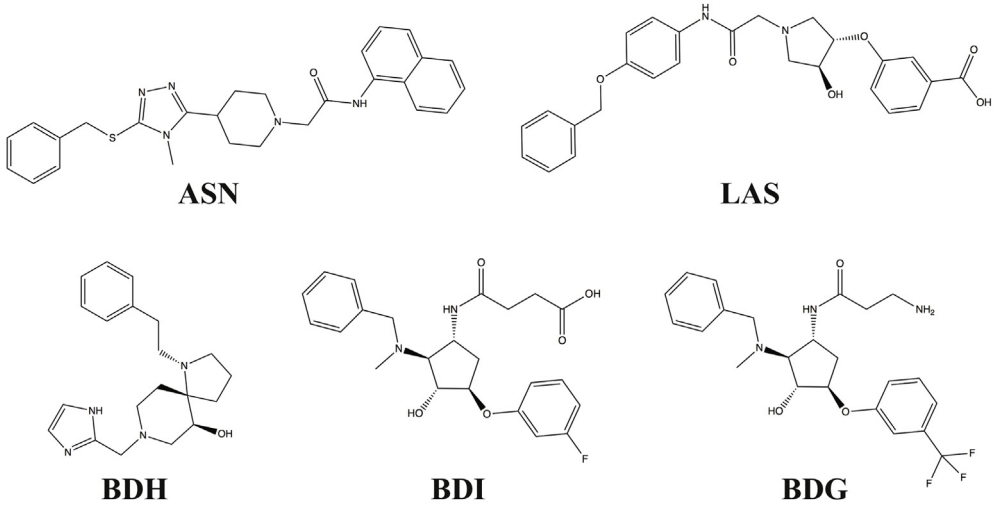

Fig. 4. Commercially available compounds from Asinex selected for *in vitro* validation from the virtual screen.

Table 1
Activity and toxicity of commercially available hits.

	IF Assay EC_{50} (μM)[a]				CC_{50} (μM)[b]
	A/WS/33 (H1N1)	A/Victoria/75 (H3N2)	A/Taiwan/ 64 (H2N2)	B/Gl/ 1739/54	
LAS	9.5 ± 0.7	9.1 ± 1.3	20 ± 7	ND[c]	389 ± 23
ASN	15 ± 2	11 ± 3	27 ± 10	26 ± 5	117 ± 20
BDG	19 ± 1	23 ± 3	25 ± 2	17 ± 3	99 ± 8.0
BDI	38 ± 6	> 50	> 50	> 50	226 ± 14
BDH	> 50	> 50	> 50	33 ± 14	402 ± 31

[a] 50% Efficacy Concentration (± standard error).
[b] 50% Cytotoxic Concentration (± standard error), or the concentration that killed 50% of cells in 72 h, measured by crystal violet uptake and retention.
[c] Not done.

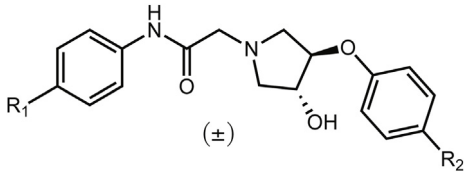

Fig. 5. LAS Derivative Template. Scaffolds for LAS analogs were made by modifying R_1 or R_2. For compound **10**, the hydroxyl group on the cyclopentyl-ring was omitted.

binding. This interaction pulls the rest of the NLS in closer to the rest of the complex. The alpha helix comprised of residues 142–152 was 54.5% conserved between IAV and IBV, but the differences were minimal. Despite these structural and sequence differences, the proposed binding pocket is highly conserved, and inhibitors designed to bind in this pocket are effective against IAV and IBV.

Several inhibitors (BDG, BDH, BDI, ASN, compounds **3**–**7**) were tested for influenza polymerase inhibition in a Luciferase minigenome reporter assay using 293T cells (Ozawa et al., 2006). All but compound **6** showed no inhibition of enzyme activity up to 50 μM (data not shown), whereas Favipiravir, a well-characterized influenza polymerase inhibitor (Furuta et al., 2013), gave an IC_{50} of 17.3 μM (Table 7). Except for BDG, which had CC_{50} 25.3 μM, none were toxic (CC_{50} > 50 μM) to 293T cells in the XTT-CTX assay (data not shown), an assay that measures the toxicity by measuring the amount of metabolic activity in cells. Compound **20** showed some inhibition of polymerase activity with an IC_{50} of 51 μM in 293T cells, so it was tested in vRNP-expressing Vero and HepG2-hNTCP cells (Table 7), where it had better activity than Favipiravir. Compound **20** also had low cytotoxicity (a CC_{50} greater than 100 μM) in these cell types. However, in additional cytotoxicity tests with MT-4 and Huh-7 cells, cytotoxicity was similar to that in 293T cells.

BDI and compound **20** were tested in the XTT-CPE and plaque assays to further confirm the activity of the inhibitors (Table 8). Both compounds had comparable low micromolar EC_{50}'s and 100% inhibition achieved within the concentration ranges tested. Compound **20** showed consistent activity in both CPE assays and the Plaque assay.

The effect of compound **20** on dynamic cellular localization of PB1 and NP was determined late in the cycle for infected MDCK cells. Infected cells were treated with DMSO, importazole (IPZ), or compound **20**. PB1 or NP localization was determined by immunofluorescence, as illustrated in Fig. 7. IPZ is a small molecule inhibitor of Importin-β that served as a dynamic nuclear localization inhibition control (Soderholm et al., 2011). We refer to the localization as "dynamic" because it is clear in the previously cited work and this that nuclear import of PB1 and (here) export of NP must be ongoing even in late-stage (16 h PI) infected cells. Nuclear localization of PB1 was significantly reduced (Fig. 8A) in 50 μM compound **20**-treated cells, and the number of cells with complete cytoplasmic localization was increased in the IPZ and compound **20**-treated cells. The pattern for PB1 localization when treated with compound **20** closely resembles the pattern observed previously (Fodor and Smith, 2004) when the nuclear localization sequence was deleted from PB1. NP was found primarily in the cytoplasm of the cell in vehicle controls, which is consistent with previous results (Frensing et al., 2016). However, the localization of NP was dramatically affected by compound **20** treatment (Fig. 8B). The treatment caused most cells to have nuclear localization of NP. A similar effect was observed for IPZ-treated cells, suggesting that blocking nuclear import of PB1 perturbs nuclear export of NP.

4. Discussion

Several groups have shown the utility of using virtual screening to design novel inhibitors of a protein target (Busschots et al., 2012; Geppert et al., 2011, 2012; Shima et al., 2013). In many cases, the binding site is well defined, and the binding of known inhibitors can inform further optimization (Hoi et al., 2015; Mitrasinovic, 2013; Zhao and Caflisch, 2015). In this study, we docked a focused library of protein-protein interaction inhibitors to a previously uncharacterized binding site candidate near PB1's bipartite nuclear localization signal. It is a PB2-PB1 interaction site and is also a predicted interface between PB1 and RanBP5. Small-angle x-ray scattering data showed that the overall shape of PB1-PA did not change much upon binding to RanBP5.

Table 2
Structure-activity relationship of LAS-Derivatives with A/WS/33 (H1N1).

ID#	R_1	R_2	IF EC_{50} (μM)[a]	CV-CPE EC_{50} (μM)[a]	CV CTX CC_{50} (μM)[b]	SI[c]
LAS[d]	OBn	(m)-COOH	9.5 ± 0.7	ND[f]	389 ± 23	ND
1	OBn	(m)-COOH	> 50	*No Effect*	160 ± 5	< 1
2	OBn	(m)-COOMe	15 ± 3	*No Effect*	86 ± 10	< 1
3	OBn	COOH	25 ± 6	*No Effect*	210 ± 20	< 1
4	OBn	COOMe	0.95 ± 0.4	*No Effect*	52 ± 12	< 1
5	OBn	CH_2COOH	5.5 ± 1.5	*No Effect*	260 ± 60	< 1
6	OBn	CH_2COOMe	0.76 ± 0.1	*No Effect*	51 ± 9	< 1
7	OBn	CH_2CH_2COOH	38 ± 2	*No Effect*	> 200	< 1
8	OBn	CH_2CH_2COOMe	21 ± 5	*No Effect*	> 100	< 1
9	OBn	$CH_2CONHMe$	2.8 ± 0.2	*No effect*	99 ± 2	< 1
10	OBn	CH_2COOMe	2.3 ± 0.7	ND	8.9 ± 1.0	ND
11	OMe	CH_2COOMe	> 20	*No Effect*	> 100	< 1
12	FuranPh	CH_2COOMe	2.9 ± 0.2	ND	150 ± 13	ND
13	NHCOPh	CH_2COOMe	12 ± 2	ND	18 ± 1	ND
14	(m)-OBn	CH_2COOMe	12.0 ± 0.7	ND	64 ± 4	ND
15	OPh	CH_2COOMe	35 ± 4	ND	19 ± 1	ND
16	(m)-OPh	CH_2COOMe	15 ± 2	ND	35 ± 1	ND
17	(o)-OPh	CH_2COOMe	19 ± 5	ND	86 ± 12	ND
18	(m)-ONaph	CH_2COOMe	27 ± 3	> 60	48 ± 1	< 1
19	ONaph	CH_2COOMe	> 50	ND	43 ± 2	ND
20	OBnCN	CH_2COOMe	0.12 ± 0.02	8.7 ± 1.6	56 ± 18	6.4
21	OBnCl	CH_2COOMe	0.08 ± 0.02	18.9 ± 0.8	> 100	> 7.9
22	$OBnCF_3$	CH_2COOMe	0.28 ± 0.04	5.2 ± 0.01	8.4 ± 0.7	1.6
23	OBnMe	CH_2COOMe	0.8 ± 0.1	ND	50 ± 7	ND
24	OBnOMe	CH_2COOMe	> 10	ND	92 ± 80	ND
Rb[e]	NA	NA	6.6 ± 0.6	65.0 ± 0.2	ND	ND

[a] 50% Effective Concentration (+/- standard error).
[b] 50% Cytotoxic Concentration (+/- standard error).
[c] Selectivity Index: CV-CTX CC_{50}/CV-CPE EC_{50}.
[d] LAS was purchased from Asinex. Compounds 1–24 were synthesized for this study.
[e] Ribavirin.
[f] ND: Not Done.

Table 3
Immunofluorescence results against multiple strains.

IF Assay EC_{50} (μM)[a]					
ID#	A/WS/33 (H1N1)	A/CA/09 (H1N1)	A/Taiwan/64 (H2N2)	A/Victoria/75 (H3N2)	B/Gl/54
6	0.8 ± 0.1	1.3 ± 0.5	2.4 ± 0.3	2.0 ± 0.4	0.7 ± 0.2
18	27 ± 3	20 ± 3	2.3 ± 0.8	22 ± 7	15 ± 2
20	0.12 ± 0.02	0.26 ± 0.04	0.18 ± 0.02	0.42 ± 0.08	0.38 ± 0.03
21	0.08 ± 0.02	0.008 ± 0.002	0.031 ± 0.005	0.10 ± 0.02	0.23 ± 0.03

[a] 50% Effective Concentration (+/- standard error).

Table 4
Crystal violet CPE results against multiple strains.

CV-CPE EC_{50} (μM)[a]					
ID#	A/WS/33 (H1N1)	A/CA/09 (H1N1)	A/Taiwan/ 64 (H2N2)	A/Victoria/ 75 (H3N2)	B/Gl/54
6	*No effect*	*No effect*	12 ± 3	> 80	32 ± 1
18	> 60	*No effect*	53 ± 0.5	*No effect*	74 ± 6
20	8.7 ± 1.6	3.7 ± 0.3	5.7 ± 0.6	44 ± 1	12.4 ± 0.5
21	18.9 ± 0.8	13.5 ± 0.6	4.7 ± 0.7	> 80	14 ± 2

[a] 50% Effective Concentration (+/- standard error).

Table 5
Resistance development for ASN and compound 20.

Passage [a]	ASN IF Assay EC_{50} (μM)[b]	Compound **20** IF Assay EC_{50} (μM)[b]
0	11 ± 3	$0.12 \pm {}^{0.02}$
5	23 ± 2	0.17 ± 0.02
10	> 50	0.109 ± 0.007

[a] Passaging began with A/Victoria/3/75 (against ASN) or A/WS/33 (against **20**). For each passage, MDCK cells were infected in the presence of ASN or **20** and monitored for CPE.
[b] 50% Effective Concentration (± standard error).

However, the shape of RanBP5 changed significantly upon binding to the PB1-PA heterodimer (Swale et al., 2016). Current knowledge of the PB1-PA/RanBP5 interaction is limited to biochemical data and computational models. In our simulations, the crystal structures of PB1-PA and Kap121p, a RanBP5 homologue, could be readily docked as rigid structures with excellent interface complementarity, and the selected site appeared to be well suited to interfere with complexation (Fig. 2A and B).

In general, the LAS derivatives were more effective in the IF assay than they were in the XTT-CPE or CV-CPE assays. For a virus like influenza, where the number of progeny is ~2000 per infected cell (Frensing et al., 2016), a drug has to block infection very strongly (99.95%) to prevent complete cell culture death for 5 generations, especially if the multiplicity of infection is reasonably high, e.g. 0.1 infectious particles per cell, in the initial infection. The IF assay is a useful tool in screening and optimizing polymerase inhibitors because of its sensitivity and short duration, which allows for minimal exposure of cultured cells to the toxic effects of the compounds. Compound **20**

Table 6
IAV and IBV multiple sequence alignments.

Res#[a]	142	143	144	145	146	147	148	149	150	151	152
IAV AAs[b]	A	L	A[d]	N[d]	T	I	E[d]	V	F	R[d]	K[d]
f [c]	0.999	0.999	0.998	0.999	0.999	0.999	0.999	0.916	0.999	0.994	0.934
IBV AAs	A	L	N	T	T	I	T	S	F	R	L
Res#[e]	679[b]	680	681	682	683	684	685	686	687	688	689
IAV AAs	Q	R[d]	G[d]	I	L	E	D[d]	E	R	I	Y[d]
f	0.999	0.994	0.999	0.990	0.997	0.999	0.999	0.999	0.988	0.997	0.999
IBV AAs	Q	R	N	M	I	L	E	E	Q	C	Y

[a] IAV numbering.
[b] Amino acids, single letter code.
[c] If represents the frequency of the amino acids for all of the unique sequences of IAV.
[d] Represents residues that have side chains projecting towards/into the proposed binding pocket.
[e] IAV numbering; For IBV, the numbering starts at 680 and ends at 690.

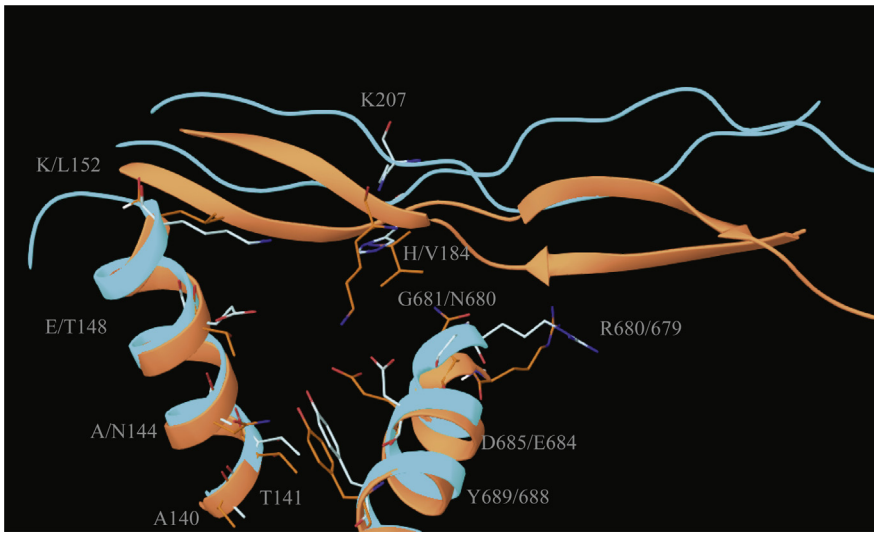

Fig. 6. Alignment of IAV PB1 (turquoise, 4WSB) and IBV PB1 (orange, 4WSA). Binding site residue side chains are displayed with the stick representation. D685 in IAV is a glutamate in IBV. The longer side chain in IBV results in an interaction with K207 of the NLS that pulls it closer into the pocket, making the proposed binding site potentially more crowded. The secondary structure and most residues in this region of PB1 are structurally well-conserved. (For interpretation of the references to colour in this figure legend, the reader is referred to the Web version of this article.)

Table 7
Polymerase inhibition assay results.

Cell type	**20** IC_{50} (μM)[a]	**20** CC_{50} (μM)[b]	Favipiravir IC_{50} (μM)[a]
293T	51 (42–62)	3.1 (2.7–3.6)	17.3 (12.2–24.6)
Vero	1.20 (0.55–2.7)	> 100	3.0 (1.3–7.0)
HepG2-hNTCP	29 (18–45)	> 100	62.0 (22–176)
MT-4	ND	18.4 (15.9–21.5)	ND
Huh7	ND	3.4 (2.3–4.8)	ND

[a] Flu Pol Assay.
[b] XTT Assay. 95% confidence intervals are in parentheses. ND: Not done.

Table 8
XTT CPE and plaque assay results.

Compound	XTT-CPE EC_{50} (μM)[a]	Plaque EC_{50} (μM)[a]
BDI	7.2 (4.8–10.7)	5.7 (4.0–8.3)
20	5.9 (5.5–6.3)	9.9 (8.3–11.8)
Favipiravir	15.2 (12.5–18.5)	11.2 (7.5–16.5)

[a] The virus used in both assays was A/CA/09. The uncertainty is represented by the 95% confidence interval.

was the most effective compound in the CV-CPE assay, so it was the focus of further characterization in this work. Other compounds, including compound **21** and BDI, also had promising activity and will be studied further.

Compound **20** showed high variability in toxicity depending on the cell line used (Table 7). This suggests that there is alternative-target activity that is specific to certain cell lines.

Resistance developed slowly against ASN. After ten passages, very little activity for ASN was observed at 50 μM (Table 5). Resistance developed even more slowly against compound **20**. After ten passages, no detectable resistance was observed with the IF assay, suggesting that the target for influenza virus inhibition is highly conserved and difficult for the virus to escape.

Compound **20** was shown to block the IAV polymerase in three cell lines with the luciferase reporter assay. In two cases, compound **20** was more effective against the polymerase than the well-characterized polymerase inhibitor Favipiravir, which is approved for human usage in Japan (Furuta et al., 2017). The variation of IC_{50} values between cell lines is most likely due to transfection efficiency. This data shows that some aspect of polymerase function is being perturbed, which could include the nuclear import, complex assembly, or accurate transcription of mRNA.

NP and PB1 are expected to be dispersed throughout the infected cells at the time of inhibitor addition. Our results of late stage localization are consistent with localization being a dynamic process, even at this late point in the infection, and we interpret our results in this context. The PB1 localization data strongly suggests that compound **20** destabilizes a protein-protein interaction that is important for PB1 nuclear import. This could be the PB1-PA interaction or the PB1-PA-RanBP5 interaction. Direct binding of inhibitors to RanBP5 was not ruled out in this study. PB1 localization in cells treated with compound **20** closely resembled the phenotype observed when the bipartite

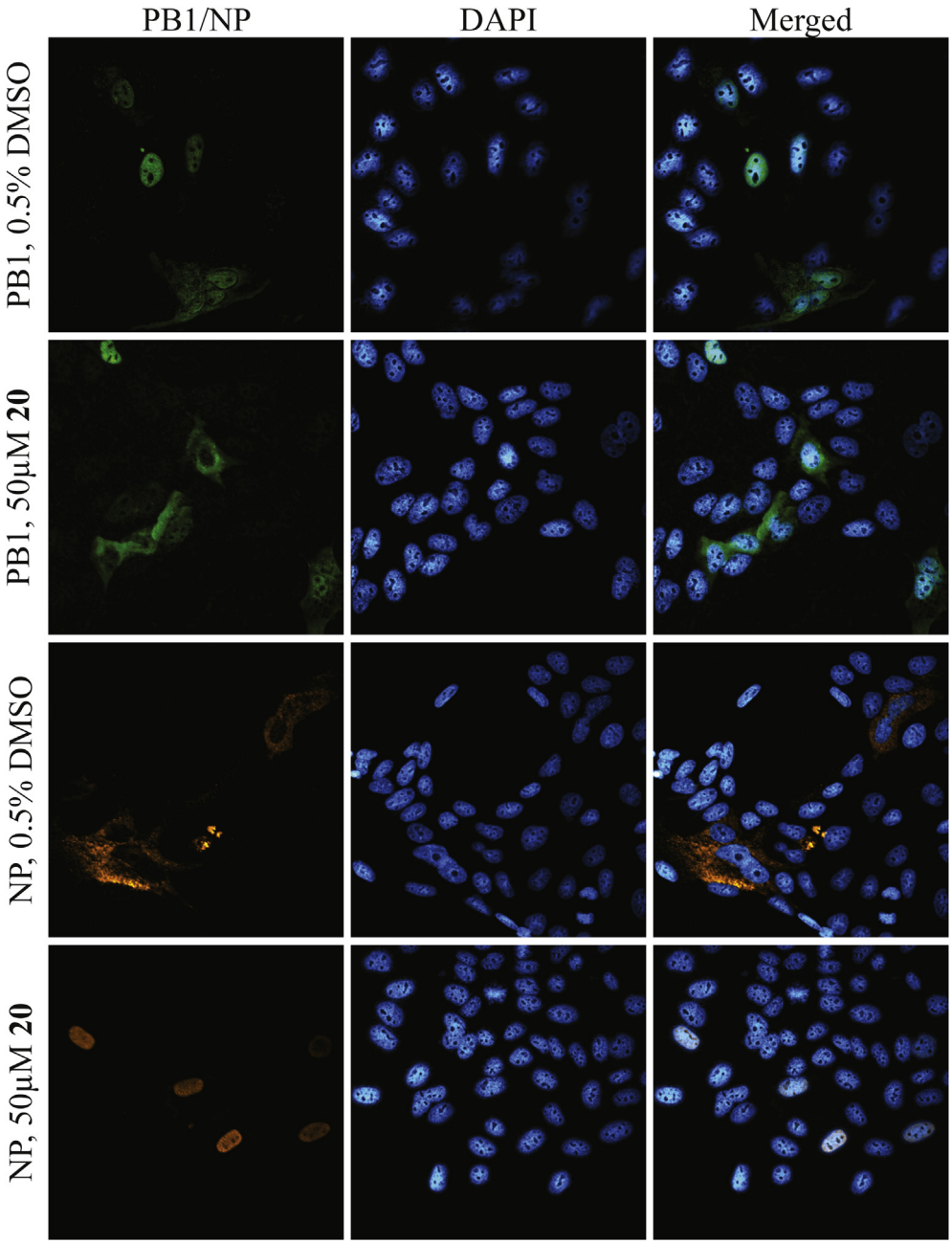

Fig. 7. Representative images for each condition used in the PB1 localization assay. Detection of PB1 (green) or NP (orange) was carried out in infected MDCK cells at 17 h post infection with DAPI (cyan) as a counterstain. (For interpretation of the references to colour in this figure legend, the reader is referred to the Web version of this article.)

nuclear localization signal was removed from PB1 (Hutchinson et al., 2011). This phenotype also matched the IPZ-treated cells, which served as a nuclear import inhibition control (Soderholm et al., 2011). In fact, compound **20** had a much larger impact than IPZ on PB1 localization. Though the binding site and exact mechanism of inhibition remain unproven, the activity of the compounds was confirmed in five assays.

Disrupting PB1 nuclear import perturbed NP localization as well, as after one hour of inhibitor treatment the majority of NP had become localized in the nucleus (Fig. 8B). Treatment with IPZ abolished cytoplasmic NP localization, and treatment with compound **20** caused 73% of the cells to have nuclear localization. This dramatic change could be explained by the mechanism of vRNP export. By preventing nuclear accumulation of PB1, NP export in conjunction with PB1 in vRNPs is indirectly, but effectively blocked by IPZ and compound **20**.

Future work should include expressing and purifying the PB1/PA complex allowing determination of binding affinities and crystallographic structure for complexes with the compounds bound. Assays to determine the destabilization of protein complexes could be carried out to determine the exact mechanism of action on the polymerase. If the selectivity index can be increased, animal testing could be conducted. Additional passaging combined with isolation of resistant strains and sequence analysis will give further insights into the resistance potential and fitness costs associated with escape mutations. Resistant sequences should be compared to more comprehensive sequence databases, like GISAID, to determine the prevalence of relevant mutants. Nuclear import inhibitors could one day serve as a promising therapy to complement currently available influenza treatments and other therapies that are in development.

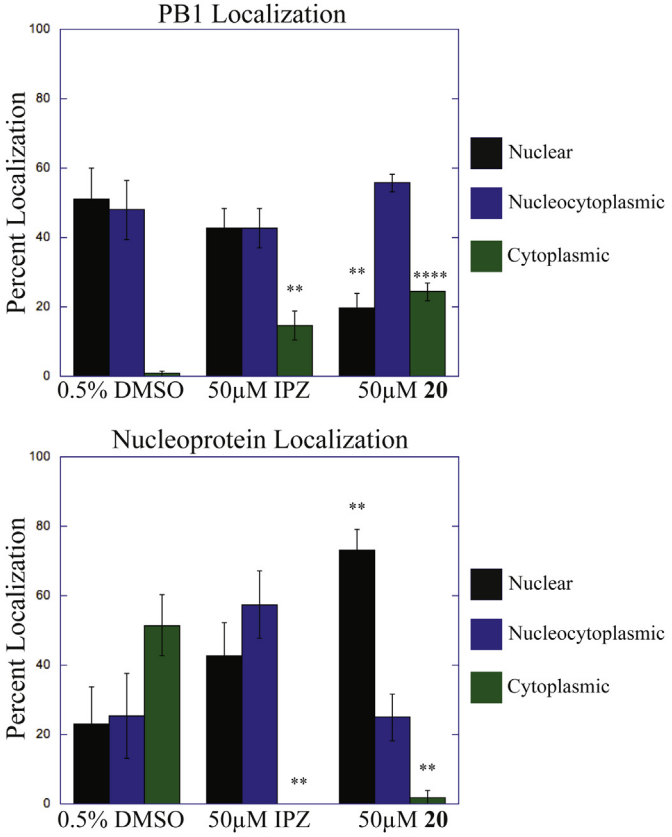

Fig. 8. Effect of compound **20** on PB1 Nuclear Localization. **A)** Classification of PB1 localization in infected cells treated with 0.5% DMSO (105 infected cells, 10 images), 50 μM IPZ (119 infected cells, 12 images), or 50 μM compound **20** (172 infected cells, 11 images). **B)** Classification of NP localization in infected cells treated with 0.5% DMSO (50 infected cells, 5 images), 50 μM IPZ (76 infected cells, 5 images), or 50 μM compound **20** (51 infected cells, 4 images). Each condition was done in duplicate. Error bars indicate the standard error of the mean. Black bars are the percent of cells with nuclear localization of PB1 or NP. Blue refers to cells with nucleocytoplasmic localization. Green refers to cells with cytoplasmic localization. * signifies $p < 0.05$, ** signifies $p < 0.01$, **** signifies $p < 0.0001$. Each p-value compares the percent of cells under the condition to that under the equivalent condition in the 0.5% DMSO-treated cells. Nuclear localization behaves oppositely for the two proteins: IPZ and compound **20** enhance NP while reducing PB1 nuclear localization. (For interpretation of the references to colour in this figure legend, the reader is referred to the Web version of this article.)

Acknowledgements

This research did not receive any specific grant from funding agencies in the public, commercial, or not-for-profit sectors. The authors would like to acknowledge Nicole Nelson and Mackenzie Williamson from the Busath lab for their help with CPE assays. We thank Milan Kožíšek, Jakub Hejdánek, Elena Karlukova, and Jan Konvalinka from the Institute of Organic Chemistry and Biochemistry, Czech Academy of Sciences and Brad Berges and R. Paul Evans from the Brigham Young University Microbiology Department for consultations on the project.

Appendix A. Supplementary data

Supplementary data to this article can be found online at https://doi.org/10.1016/j.antiviral.2019.02.003.

References

Busschots, K., Lopez-Garcia, L.A., Lammi, C., Stroba, A., Zeuzem, S., Piiper, A., Alzari, P.M., Neimanis, S., Arencibia, J.M., Engel, M., Schulze, J.O., Biondi, R.M., 2012. Substrate-Selective inhibition of protein kinase PDK1 by small compounds that bind to the PIF-pocket allosteric docking site. Chem. Biol. 19, 1152–1163.
Chase, G., Deng, T., Fodor, E., Leung, B.W., Mayer, D., Schwemmle, M., Brownlee, G., 2008. Hsp90 inhibitors reduce influenza virus replication in cell culture. Virology 377, 431–439.
Comeau, S.R., Gatchell, D.W., Vajda, S., Camacho, C.J., 2004. ClusPro: a fully automated algorithm for protein-protein docking. Nucleic Acids Res. 32, W96–W99.
Desantis, J., Nannetti, G., Massari, S., Barreca, M.L., Manfroni, G., Cecchetti, V., Palu, G., Goracci, L., Loregian, A., Tabarrini, O., 2017. Exploring the cycloheptathiophene-3-carboxamide scaffold to disrupt the interactions of the influenza polymerase subunits and obtain potent anti-influenza activity. Eur. J. Med. Chem. 138, 128–139.
Dong, G., Peng, C., Luo, J., Wang, C., Han, L., Wu, B., Ji, G., He, H., 2015. Adamantane-resistant influenza a viruses in the world (1902-2013): frequency and distribution of M2 gene mutations. PLoS One 10, e0119115.
Fodor, E., Smith, M., 2004. The PA subunit is required for efficient nuclear accumulation of the PB1 subunit of the influenza A virus RNA polymerase complex. J. Virol. 78, 9144–9153.
Frensing, T., Kupke, S.Y., Bachmann, M., Fritzsche, S., Gallo-Ramirez, L.E., Reichl, U., 2016. Influenza virus intracellular replication dynamics, release kinetics, and particle morphology during propagation in MDCK cells. Appl. Microbiol. Biotechnol. 100, 7181–7192.
Friesner, R.A., Banks, J.L., Murphy, R.B., Halgren, T.A., Klicic, J.J., Mainz, D.T., Repasky, M.P., Knoll, E.H., Shelley, M., Perry, J.K., Shaw, D.E., Francis, P., Shenkin, P.S., 2004. Glide: a new approach for rapid, accurate docking and scoring. 1. Method and assessment of docking accuracy. J. Med. Chem. 47, 1739–1749.
Friesner, R.A., Murphy, R.B., Repasky, M.P., Frye, L.L., Greenwood, J.R., Halgren, T.A., Sanschagrin, P.C., Mainz, D.T., 2006. Extra precision glide: docking and scoring incorporating a model of hydrophobic enclosure for protein-ligand complexes. J. Med. Chem. 49, 6177–6196.
Furuta, Y., Gowen, B.B., Takahashi, K., Shiraki, K., Smee, D.F., Barnard, D.L., 2013. Favipiravir (T-705), a novel viral RNA polymerase inhibitor. Antivir. Res. 100, 446–454.
Furuta, Y., Komeno, T., Nakamura, T., 2017. Favipiravir (T-705), a broad spectrum inhibitor of viral RNA polymerase. Proc. Jpn. Acad. Ser. B Phys. Biol. Sci. 93, 449–463.
Geppert, T., Bauer, S., Hiss, J.A., Conrad, E., Reutlinger, M., Schneider, P., Weisel, M., Pfeiffer, B., Altmann, K.H., Waibler, Z., Schneider, G., 2012. Immunosuppressive small molecule discovered by structure-based virtual screening for inhibitors of protein-protein interactions. Angew. Chem. Int. Ed. 51, 258–261.
Geppert, T., Reisen, F., Bauer, S., Hoy, B., Batista-Perez, T., Pfeiffer, B., Wessler, S., Waibler, Z., Schneider, G., 2011. iPred: from interface prediction to actual inhibitors of protein-protein interaction. Abstr. Pap. Am. Chem. Soc. 242.
Halgren, T.A., Murphy, R.B., Friesner, R.A., Beard, H.S., Frye, L.L., Pollard, W.T., Banks, J.L., 2004. Glide: a new approach for rapid, accurate docking and scoring. 2. Enrichment factors in database screening. J. Med. Chem. 47, 1750–1759.
Hensley, S.E., 2014. Challenges of selecting seasonal influenza vaccine strains for humans with diverse pre-exposure histories. Curr. Opin. Virol. 8, 85–89.
Hoi, P.M., Li, S., Vong, C.T., Tseng, H.H., Kwan, Y.W., Lee, S.M., 2015. Recent advances in structure-based drug design and virtual screening of VEGFR tyrosine kinase inhibitors. Methods 71, 85–91.
Hoopes, J.D., Driebe, E.M., Kelley, E., Engelthaler, D.M., Keim, P.S., Perelson, A.S., Rong, L., Went, G.T., Nguyen, J.T., 2011. Triple combination antiviral drug (TCAD) composed of amantadine, oseltamivir, and ribavirin impedes the selection of drug-resistant influenza A virus. PLoS One 6, e29778.
Hussain, M., Galvin, H.D., Haw, T.Y., Nutsford, A.N., Husain, M., 2017. Drug resistance in influenza A virus: the epidemiology and management. Infect. Drug Resist. 10, 121–134.
Hutchinson, E.C., Fodor, E., 2013. Transport of the influenza virus genome from nucleus to nucleus. Viruses 5 (10), 2424–2446.
Hutchinson, E.C., Orr, O.E., Man Liu, S., Engelhardt, O.G., Fodor, E., 2011. Characterization of the interaction between the influenza A virus polymerase subunit PB1 and the host nuclear import factor Ran-binding protein 5. J. Gen. Virol. 92, 1859–1869.
Jones, J.C., Kumar, G., Barman, S., Najera, I., White, S.W., Webby, R.J., Govorkova, E.A., 2018. Identification of the I38T PA substitution as a resistance marker for next-generation influenza virus endonuclease inhibitors. mBio 9 (2) e00430-18.
Kobayashi, J., Matsuura, Y., 2013. Structural basis for cell-cycle-dependent nuclear import mediated by the karyopherin Kap121p. J. Mol. Biol. 425, 1852–1868.
Kolocouris, A., Tzitzoglaki, C., Johnson, F.B., Zell, R., Wright, A.K., Cross, T.A., Tietjen, I., Fedida, D., Busath, D.D., 2014. Aminoadamantanes with persistent in vitro efficacy against H1N1 (2009) influenza A. J. Med. Chem. 57, 4629–4639.
Kozakov, D., Hall, D.R., Xia, B., Porter, K.A., Padhorny, D., Yueh, C., Beglov, D., Vajda, S., 2017. The ClusPro web server for protein-protein docking. Nat. Protoc. 12, 255–278.
Li, C., Wang, Z., Cao, Y., Wang, L., Ji, J., Chen, Z., Deng, T., Jiang, T., Cheng, G., Qin, F.X., 2017. Screening for novel small-molecule inhibitors targeting the assembly of influenza virus polymerase complex by a bimolecular luminescence complementation-based reporter system. J. Virol. 91.
Massari, S., Goracci, L., Desantis, J., Tabarrini, O., 2016. Polymerase acidic protein-basic protein 1 (PA-PB1) protein-protein interaction as a target for next-generation anti-influenza therapeutics. J. Med. Chem. 59, 7699–7718.
McKimm-Breschkin, J.L., 2000. Resistance of influenza viruses to neuraminidase inhibitors —a review. Antivir. Res. 47, 1–17.

McKimm-Breschkin, J.L., Jiang, S., Hui, D.S., Beigel, J.H., Govorkova, E.A., Lee, N., 2018. Prevention and treatment of respiratory viral infections: presentations on antivirals, traditional therapies and host-directed interventions at the 5th ISIRV Antiviral Group conference. Antivir. Res. 149, 118–142.

Mitrasinovic, P.M., 2013. Progress in structure-based design of EGFR inhibitors. Curr. Drug Targets 14, 817–829.

Molinari, N.A., Ortega-Sanchez, I.R., Messonnier, M.L., Thompson, W.W., Wortley, P.M., Weintraub, E., Bridges, C.B., 2007. The annual impact of seasonal influenza in the US: measuring disease burden and costs. Vaccine 25, 5086–5096.

Muratore, G., Goracci, L., Mercorelli, B., Foeglein, Á., Digard, P., Cruciani, G., Palù, G., Loregian, A., 2012. Small molecule inhibitors of influenza A and B viruses that act by disrupting subunit interactions of the viral polymerase. Proc. Natl. Acad. Sci. U. S. A. 109 (16), 6247–6252.

Noshi, T., Kitano, M., Taniguchi, K., Yamamoto, A., Omoto, S., Baba, K., Hashimoto, T., Ishida, K., Kushima, Y., Hattori, K., Kawai, M., Yoshida, R., Kobayashi, M., Yoshinaga, T., Sato, A., Okamatsu, M., Sakoda, Y., Kida, H., Shishido, T., Naito, A., 2018. In vitro characterization of baloxavir acid, a first-in-class cap-dependent endonuclease inhibitor of the influenza virus polymerase PA subunit. Antivir. Res. 160, 109–117.

Ortigoza, M.B., Dibben, O., Maamary, J., Martinez-Gil, L., Leyva-Grado, V.H., Abreu Jr., P., Ayllon, J., Palese, P., Shaw, M.L., 2012. A novel small molecule inhibitor of influenza A viruses that targets polymerase function and indirectly induces interferon. PLoS Pathog. 8, e1002668.

Ozawa, M., Fujii, K., Muramoto, Y., Yamada, S., Yamayoshi, S., Takada, A., Goto, H., Horimoto, T., Kawaoka, Y., 2006. Contributions of two nuclear localization signals of influenza A virus nucleoprotein to viral replication. J. Virol. 81 (1), 30–41.

Perwitasari, O., Johnson, S., Yan, X.Z., Howerth, E., Shacham, S., Landesman, Y., Baloglu, E., McCauley, D., Tamir, S., Tompkins, S.M., Tripp, R.A., 2014. Verdinexor, a novel selective inhibitor of nuclear export, reduces influenza a virus replication in vitro and in vivo. J. Virol. 88, 10228–10243.

Reich, S., Guilligay, D., Pflug, A., Malet, H., Berger, I., Crepin, T., Hart, D., Lunardi, T., Nanao, M., Ruigrok, R.W., Cusack, S., 2014. Structural insight into cap-snatching and RNA synthesis by influenza polymerase. Nature 516, 361–366.

Resa-Infante, P., Paterson, D., Bonet, J., Otte, A., Oliva, B., Fodor, E., Gabriel, G., 2015. Targeting importin-alpha7 as a therapeutic approach against pandemic influenza viruses. J. Virol. 89, 9010–9020.

Schmidtke, M., Schnittler, U., Jahn, B., Dahse, H., Stelzner, A., 2001. A rapid assay for evaluation of antiviral activity against coxsackie virus B3, influenza virus A, and herpes simplex virus type 1. J. Virol Methods 95, 133–143.

Scudiero, D.A., Shoemaker, R.H., Paull, K.D., Monks, A., Tierney, S., Nofziger, T.H., Currens, M.J., Seniff, D., Boyd, M.R., 1988. Evaluation of a soluble tetrazolium/formazan assay for cell growth and drug sensitivity in culture using human and other tumor cell lines. Cancer Res. 48, 4827–4833.

Shima, F., Yoshikawa, Y., Ye, M., Araki, M., Matsumoto, S., Liao, J.L., Hu, L.Z., Sugimoto, T., Ijiri, Y., Takeda, A., Nishiyama, Y., Sato, C., Muraoka, S., Tamura, A., Osoda, T., Tsuda, K., Miyakawa, T., Fukunishi, H., Shimada, J., Kumasaka, T., Yamamoto, M., Kataoka, T., 2013. In silico discovery of small-molecule Ras inhibitors that display antitumor activity by blocking the Ras-effector interaction. Proc. Natl. Acad. Sci. U.S.A. 110, 8182–8187.

Soderholm, J.F., Bird, S.L., Kalab, P., Sampathkumar, Y., Hasegawa, K., Uehara-Bingen, M., Weis, K., Heald, R., 2011. Importazole, a small molecule inhibitor of the transport receptor importin-beta. ACS Chem. Biol. 6, 700–708.

Su, C.Y., Cheng, T.J., Lin, M.I., Wang, S.Y., Huang, W.I., Lin-Chu, S.Y., Chen, Y.H., Wu, C.Y., Lai, M.M., Cheng, W.C., Wu, Y.T., Tsai, M.D., Cheng, Y.S., Wong, C.H., 2010. High-throughput identification of compounds targeting influenza RNA-dependent RNA polymerase activity. Proc. Natl. Acad. Sci. U. S. A. 107, 19151–19156.

Swale, C., Monod, A., Tengo, L., Labaronne, A., Garzoni, F., Bourhis, J.M., Cusack, S., Schoehn, G., Berger, I., Ruigrok, R.W., Crepin, T., 2016. Structural characterization of recombinant IAV polymerase reveals a stable complex between viral PA-PB1 heterodimer and host RanBP5. Sci. Rep. 6, 24727.

Trott, O., Olson, A.J., 2010. AutoDock Vina: improving the speed and accuracy of docking with a new scoring function, efficient optimization, and multithreading. J. Comput. Chem. 31, 455–461.

Wutzler, P., Sauerbrei, A., Klocking, R., Brogmann, B., Reimer, K., 2002. Virucidal activity and cytotoxicity of the liposomal formulation of povidone-iodine. Antivir. Res. 54, 89–97.

Wu, W.W., Panté, N., 2009. The directionality of the nuclear transport of the influenza A genome is driven by selective exposure of nuclear localization sequences on nucleoprotein. Virol. J. 6, 68.

Zhang, J., Hu, Y., Foley, C., Wang, Y., Musharrafieh, R., Xu, S., Zhang, Y., Ma, C., Hulme, C., Wang, J., 2018. Exploring ugi-azide four-component reaction products for broad-spectrum influenza antivirals with a high genetic barrier to drug resistance. Sci. Rep. 8 (1), 4653.

Zhao, H., Caflisch, A., 2015. Molecular dynamics in drug design. Eur. J. Med. Chem. 91, 4–14.